THE JOURNAL OF PHYSICAL CHEMISTRY C
A JOURNAL OF THE AMERICAN CHEMICAL SOCIETY

pubs.acs.org/JPCC

Article

Application of High-Resolution ^{95}Mo Solid State NMR Spectroscopy in Structural Studies of Complex Alkali Molybdate Crystals and Glasses

Sabyasachi Sen,* Ivan Hung, Jacob M. Lovi, and Zhehong Gan

Cite This: *J. Phys. Chem. C* 2025, 129, 6869–6881

Read Online

ACCESS | Metrics & More | Article Recommendations

ABSTRACT: The Mo−O coordination environment is probed in a series of simple and complex crystalline alkali molybdates as well as in mixed-alkali molybdate glasses using high-field (18.8 and 20.0 T) ^{95}Mo magic-angle-spinning (MAS) and multiple-quantum MAS (MQMAS) nuclear magnetic resonance (NMR) spectroscopy. When taken together, the ^{95}Mo NMR spectroscopic results indicate that somewhat contrary to the conventional wisdom the corner- and edge-shared MoO_6 octahedral sites in these alkali molybdates are characterized by higher values of the isotropic shift (δ_{iso}) and quadrupolar coupling constant (C_Q) compared to the MoO_4 tetrahedral sites. These trends are hypothesized to be related to the unusually strong distortion of MoO_6 octahedra in corner- and edge-shared configurations and the resulting increase in the paramagnetic component of the chemical shift. While the ^{95}Mo C_Q of the MoO_4 sites displays an approximately linear positive correlation with the degree of tetrahedral distortion, no such correlation is observed for the MoO_6 sites. High-resolution ^{95}Mo NMR spectra show the coexistence of tetrahedral and octahedral Mo−O environments in the structure of alkali molybdate glasses, with the relative fraction of the latter environment increasing with Mo content. The results presented in this study indicate that high-resolution ^{95}Mo NMR spectroscopy at high magnetic fields (∼20 T or higher) may prove to be a promising tool for investigating the Mo−O coordination environments in nuclear waste glasses.

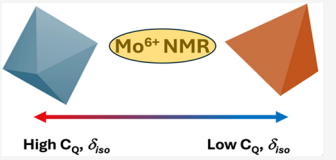

1. INTRODUCTION

Molybdenum (Mo) is an early transition metal that has found a wide range of technological applications. Mo is used as an alloying agent in steel and other metals to improve mechanical strength and resistance to corrosion and wear.[1] On the other hand, several crystalline oxide and chalcogenide compounds of Mo with high catalytic activity are utilized in various chemical processes.[2,3] It may be noted here that glasses can also be made with MoO_3 as a major constituent where, however, the glass-formation requires addition of one or more alkali oxides.[4−7] Mo is present as Mo^{6+} in these alkali molybdate glasses, where recent Raman spectroscopic studies have indicated that the structural network consists of a mixture of corner and edge-shared MoO_4 and MoO_6 polyhedra.[7] In contrast to molybdate glasses where it serves as a major component, MoO_3 is often incorporated as a minor component in silicate, borate and phosphate glasses as a nucleating agent for synthesis of glass-ceramics as well for photochromic, electrochromic and gas sensing applications where the redox behavior of Mo provides the desired functionality.[8−11]

Inorganic molybdates display rich structural chemistry where Mo is often present in multiple coordination states, predominantly as a mixture of MoO_4 tetrahedra and MoO_6 octahedra with a wide range of connectivity.[12−17] Despite its unique ability to quantitatively investigate multiple coordination states of various elements in crystal and glass structure, the application of solid-state nuclear magnetic resonance (NMR) spectroscopy of Mo has remained quite limited in the literature, owing to the rather low gyromagnetic ratio γ (-1.751×10^7 rad T^{-1} s^{-1}) and thus the low sensitivity, as well as the quadrupolar nature ($I = 5/2$) of the NMR active ^{95}Mo and ^{97}Mo nuclides. Besides, the low γ of these two nuclides also poses a problem with efficient generation of multiple quantum coherences needed for high-resolution multiple quantum magic angle spinning (MQMAS) NMR spectroscopy,[18] often desirable for acquiring high-resolution spectra of quadrupolar nuclides free of quadrupolar broadening interactions.

Performing NMR spectroscopy at high magnetic fields (≥14.1 T) is often the most effective way to address the problems associated with low-γ nuclides such as ^{95}Mo. A few such studies have indeed been reported in the literature over the last two decades.[18−20] Most interestingly, these studies indicated the lack of any clear correlation between the ^{95}Mo isotropic chemical shift δ_{iso} and the various structural parameters associated with the Mo−O coordination environments such as the Mo−O bond length and O−Mo−O bond

Received: January 26, 2025
Revised: March 11, 2025
Accepted: March 20, 2025
Published: March 28, 2025

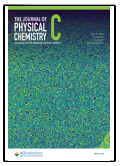

https://doi.org/10.1021/acs.jpcc.5c00614
J. Phys. Chem. C 2025, 129, 6869−6881

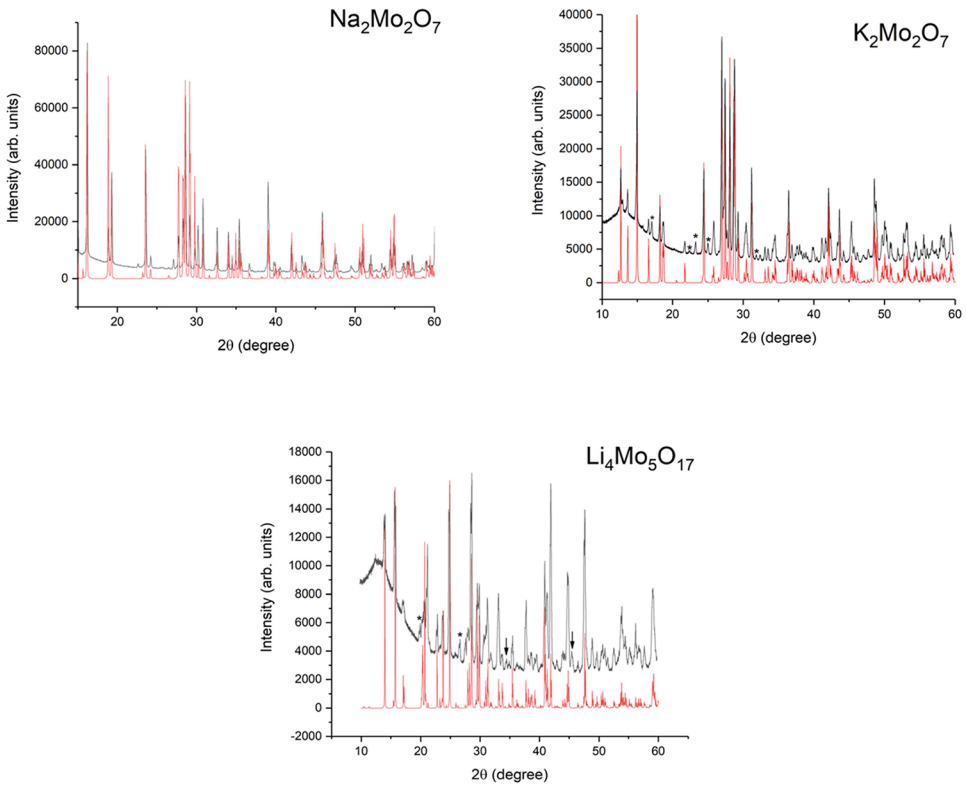

Figure 1. Experimental (black line) PXRD patterns for $Na_2Mo_2O_7$, $K_2Mo_2O_7$, and $Li_4Mo_5O_{17}$ crystals synthesized in this study. Corresponding theoretical patterns are shown as red lines. Peaks in the experimental patterns marked by asterisks and arrows are from secondary phases.

angles and their distributions as well as the Mo−O coordination numbers in these compounds, even within a given chemical series, namely the alkali molybdates.[18,19] On the other hand, a positive correlation was reported between the quadrupolar coupling constant C_Q of ^{95}Mo and the bond angle distortion factor σ for the isolated $[MoO_4]^{-2}$ tetrahedra in alkali orthomolybdates.[19] The distortion factor represents the root-mean-square deviation of these tetrahedra from T_d symmetry in terms of the root-mean-square departure of the O−Mo−O bond angles from the ideal value of 109.47° and is defined as:[19]

$$\sigma = \sqrt{\frac{1}{6}\sum_{i\neq j=1}^{6}[(\angle O_i - Mo - O_j) - 109.47^\circ]^2}$$

A similar definition for σ can be obtained for MoO_6 octahedra in terms of the departure of the 12 O−Mo−O angles between the *cis* oxygen atoms from 90°.[18] However, these pioneering studies primarily focused on alkali and alkaline-earth orthomolybdate compounds, where Mo is present in the structure as isolated and somewhat regular tetrahedral $[MoO_4]^{-2}$ anions. Only a handful of structures with Mo solely in the octahedral environment $[MoO_6]^{-6}$ have been investigated with ^{95}Mo NMR and practically no systematic NMR study of molybdates with mixed coordination states exist in the literature.[18,19] Here we utilize high-field (18.8 and 20.0 T) ^{95}Mo MAS and MQMAS NMR spectroscopy in combination with density functional theory (DFT) based calculation of ^{95}Mo quadrupolar parameters of a series of alkali molybdate crystalline compounds with Mo in coexisting tetrahedral and octahedral coordination environments with complex connectivity patterns and consequently large distortion parameters to address this gap in knowledge. It may be noted that for central transition spectra of half-integer quadrupolar nuclides such as ^{95}Mo, broadened by second-order quadrupolar effect, an increase in magnetic field results in a lowering of quadrupolar line broadening effects and an increase in resolution and sensitivity proportional to the square of the magnetic field in ppm scale.[21,22] We also report preliminary ^{95}Mo NMR results for select alkali molybdate glasses to show the feasibility of this spectroscopic technique in investigating the Mo−O coordination environments in disordered solids.

2. EXPERIMENTAL DETAILS

2.1. Sample Synthesis. The crystalline orthomolybdate phases of composition A_2MoO_4 (A = Li, Na, and K) were purchased from Aldrich (99.9%) and their phase purity was confirmed using powder X-ray diffraction (PXRD). These materials were used as received for ^{95}Mo measurements. The pyromolybdates $Na_2Mo_2O_7$ and $K_2Mo_2O_7$ as well as the polymolybdate phase $Li_4Mo_5O_{17}$ were synthesized from the corresponding melts. Stoichiometric mixtures of alkali carbonate and MoO_3 reagents (Li_2CO_3, Alfa Aesar, 99.999%; Na_2CO_3, EMD, 99.5%; K_2CO_3, Alfa Aesar, 99.997%; MoO_3, Thermo Scientific, 99.5%) were taken in silica crucible and melted at temperatures ranging between 730 and 800 °C for 20 min. The melts were transferred to another furnace and held at 420, 450, and 550 °C for 20 h, respectively, for $Li_4Mo_5O_{17}$, $K_2Mo_2O_7$, and $Na_2Mo_2O_7$ followed by cooling down to ambient temperature by turning off the furnace. The orangish yellow melts were observed to turn to opaque white crystalline material. The phase purity of the resulting materials was checked with PXRD (Figure 1). Previous studies of the

https://doi.org/10.1021/acs.jpcc.5c00614
J. Phys. Chem. C 2025, 129, 6869−6881

phase relations in the Li_2MoO_4−MoO_3 system indicate the presence of only two compounds: $Li_4Mo_5O_{17}$ and $Li_2Mo_4O_{13}$.[23] The $Na_2Mo_2O_7$ sample was found to be phase-pure, while the PXRD patterns of the $K_2Mo_2O_7$ and $Li_4Mo_5O_{17}$ phases showed the presence of small amounts of additional phases that were formed during the synthesis (Figure 1). The identity/chemistry of these secondary phases, including a small amount of residual amorphous phase, remains unclear at this point. However, the relative concentration of these secondary phases, as estimated from the PXRD patterns turns out to be rather small (5−10%) and, as discussed below, their presence does not affect the interpretation of the ^{95}Mo NMR spectra of the primary phases.

The two mixed-alkali molybdate glasses studied here were prepared using the conventional melt-quenching method. The compositions of these two glasses are 60 and 62.5 mol % MoO_3 with the remainder being a mixture of a Li_2O, Na_2O, and K_2O in a 1:1:2 molar ratio. These glasses are referred to as Mo-60 and Mo-62.5 in the subsequent discussion. Details of their synthesis can be found in a recent publication.[7] Appropriate stoichiometric mixtures of the above-mentioned alkali carbonate and MoO_3 reagents were mixed together and melted in quartz crucible in air at 730 °C for 20 min. The melts were poured onto a graphite plate and quenched by pressing with an aluminum plate. PXRD on a part of the quenched glass samples indicated the lack of any detectable crystallinity. The rest of the samples were immediately transferred and stored in a vacuum desiccator until further measurements.

2.2. ^{95}Mo NMR Spectroscopy. *2.2.1. ^{95}Mo MAS NMR at 18.8 T with Cryoprobe.* The ^{95}Mo MAS NMR spectra of the $Na_2Mo_2O_7$ crystal, the Na_2MoO_4 crystal and the Mo-60 glass were acquired at a magnetic field of 18.8 T using a Bruker Avance NEO console operating at a ^{95}Mo Larmor frequency of 52.1 MHz, and a 3.2 mm double-resonance Bruker CPMAS cryoprobe. The use of the cryoprobe resulted in excellent signal:noise ratio within a relatively short acquisition time. Crushed samples were packed into ZrO_2 rotors and spun at 6 kHz for the Na_2MoO_4 crystal and at 15 kHz for the $Na_2Mo_2O_7$ crystal and the Mo-60 glass samples. The single-pulse MAS NMR spectrum of the Na_2MoO_4 crystal was acquired using only a single scan with a $\pi/2$ pulse of duration 1.5 μs to obtain a signal:noise ratio of 250:1. Additionally, a saturation recovery experiment on Na_2MoO_4 yielded a relatively long ^{95}Mo spin−lattice relaxation time T_1 of ∼68 s, consistent with the small quadrupole moment and the cubic environment (see below) of this nuclide in this crystal. The ^{95}Mo MAS NMR spectra of the $Na_2Mo_2O_7$ crystal and the Mo-60 glass were acquired using a Hahn echo pulse sequence ($\pi/2$−τ−π-acquisition) with a $\pi/2$ pulse length of 5.5 μs and τ = 63 μs and recycle delays of 20 and 5 s for the crystal and the glass, respectively. A total of 16 scans for the crystal and 256 scans for the glass were averaged and Fourier-transformed to obtain each spectrum.

2.2.2. ^{95}Mo MAS and MQMAS at 20.0 T. The ^{95}Mo MAS and MQMAS NMR spectra of the Li_2MoO_4, K_2MoO_4, $K_2Mo_2O_7$, and $Li_4Mo_5O_{17}$ crystals and the Mo-62.5 glass were acquired at the National High Magnetic Field Laboratory (NHMFL, Tallahassee, Florida) using a Bruker Avance NEO console operating at a ^{95}Mo Larmor frequency of 55.42 MHz and a Low-E 3.2 mm HX MAS probe designed and constructed at the NHMFL. Crushed glass samples were packed into 3.2 mm ZrO_2 rotors and spun at 16 kHz. The 1D spectra of Li_2MoO_4, K_2MoO_4, and $K_2Mo_2O_7$ were acquired using a spin−echo experiment with satellite-transition saturation/inversion,[24] employing a 2 ms WURST pulse at an offset of +272,000 kHz and rf amplitude of 12.5 kHz. The QCPMG pulse sequence[25] was used instead of the spin−echo for the $Li_4Mo_5O_{17}$ crystal and Mo-62.5 glass samples for additional signal enhancement, along with the same WURST enhancement used for the other samples. $\pi/2$- and π-pulses of 4.5 and 9.0 μs were used at a rf amplitude of 18.5 kHz. The recycle delay and the number of averaged transients for each sample were: (K_2MoO_4, 65 s, 704), (Li_2MoO_4, 65 s, 1024), ($K_2Mo_2O_7$, 40 s, 2048), and ($Li_4Mo_5O_{17}$, 5 s, 2320).

The 2D spectra of $K_2Mo_2O_7$, $Li_2Mo_2O_7$ and Mo-62.5 employed a combination of triple-quantum (3Q) shifted-echo split-t_1 SPAM MQMAS[26−29] and QCPMG (Figure 2). Pulses

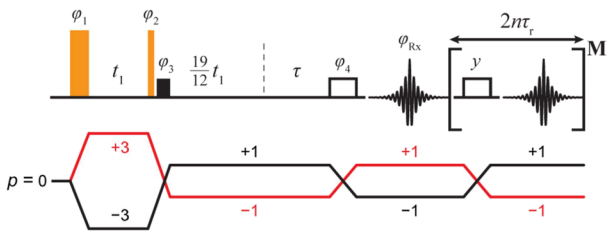

Figure 2. MQMAS/QCPMG pulse sequence used in this study with cogwheel phase cycle [26]: $\varphi_1 = 17k\cdot(2\pi/66)$, $\varphi_2 = \varphi_3 = 12k\cdot(2\pi/66)$, $\varphi_4 = 15k\cdot(2\pi/66)$, $\varphi_{Rx} = k\cdot\pi$, where k = 0, 1, 2,..., 65.

of 4.95 and 1.65 μs were used for excitation and conversion of 3Q coherence with a rf amplitude of ∼80 kHz. The indirect spectral window was rotor-synchronized by incrementing the first spli-t_1 delay by the rotor period, 62.5 μs. Hypercomplex acquisition was accomplished by incrementing the phase of the 3Q excitation pulse by 30°, as described by States et al.[30] The recycle delay, number of averaged transients, number of complex points acquired in the indirect dimension, and total experiment time for each sample were: ($K_2Mo_2O_7$, 20 s, 66, 32, 23.5 h), ($Li_4Mo_5O_{17}$, 5 s, 660, 32, 58.7 h), and (Mo-62.5, 3 s, 1518, 8, 20.2 h). In all cases using QCPMG acquisition, the echoes in the echo trains were summed prior to processing of the spectra. The ^{95}Mo chemical shift for all spectra reported here were referenced to the isotropic shift of crystalline Na_2MoO_4 at −33.5 ppm.[18]

2.3. DFT-Based Calculation of ^{95}Mo Quadrupolar Parameters. The ^{95}Mo NMR quadrupolar parameters, i.e., C_Q and the asymmetry parameter of the electric field gradient (EFG) tensor η for crystalline orthomolybdates (Li_2MoO_4, K_2MoO_4, Na_2MoO_4, $BaMoO_4$, $PbMoO_4$, and $CaMoO_4$); alkali pyromolybdates ($Na_2Mo_2O_7$ and $K_2Mo_2O_7$) and Li polymolybdate ($Li_4Mo_5O_{17}$) were calculated using the gauge-including projector augmented wave (GIPAW) method based on DFT.[31−33] The GIPAW method allows the reconstruction of the all-electron magnetic response from the pseudowave functions and is ideally suited for extended systems with periodic boundary conditions. Several past studies have demonstrated the excellent accuracy of the GIPAW method in calculating the NMR parameters for a wide variety of nuclides in crystalline and amorphous systems.[33] The NMR calculations in the present study were carried out using the code CASTEP-NMR (Biovia Inc.) within the generalized gradient approximation with Perdew−Burke−Ernzerhof (PBE) XC functionals using on-the-fly generated ultrasoft pseudopotentials and plane wave basis sets with an energy cutoff of 610 eV, where the total energy converged within 10^{-7} eV/atom.

https://doi.org/10.1021/acs.jpcc.5c00614
J. Phys. Chem. C 2025, 129, 6869−6881

Table 1. Comparison between Measured and Calculated (by DFT) ^{95}Mo Quadrupolar Parameters for Crystalline Orthomolybdate and Pyromolybdate Compounds

composition	Mo site	C_Q (measured) ± 0.05 MHz	C_Q (MHz) (calculated)	η (measured) ± 0.05	η (calculated)	structural reference
Na_2MoO_4	tetrahedral	0.0	0.0			
Li_2MoO_4	tetrahedral	1.25	1.39	0.65	0.72	
K_2MoO_4	tetrahedral	1.26	1.20	0.65	0.66	
$BaMoO_4$[a]	tetrahedral	1.68	1.79	0.10	0.00	
$PbMoO_4$[a]	tetrahedral	2.03	2.49	0.00	0.00	
$CaMoO_4$[a]	tetrahedral	2.94	3.96	0.00	0.00	
$Na_2Mo_2O_7$	tetrahedral	1.20	1.76	0.70	0.60	
	octahedral	4.10	4.84	0.80	0.75	
$K_2Mo_2O_7$	tetrahedral	2.60	3.20	0.30	0.20	
	octahedral	3.30	4.10	0.65	0.56	
$Li_4Mo_5O_{17}$	octahedral		5.76		0.39	
	octahedral		5.61		0.41	
	octahedral		5.66		0.35	
	octahedral		4.31		0.95	
	octahedral		4.35		0.49	

[a]Experimental data are from ref 18.

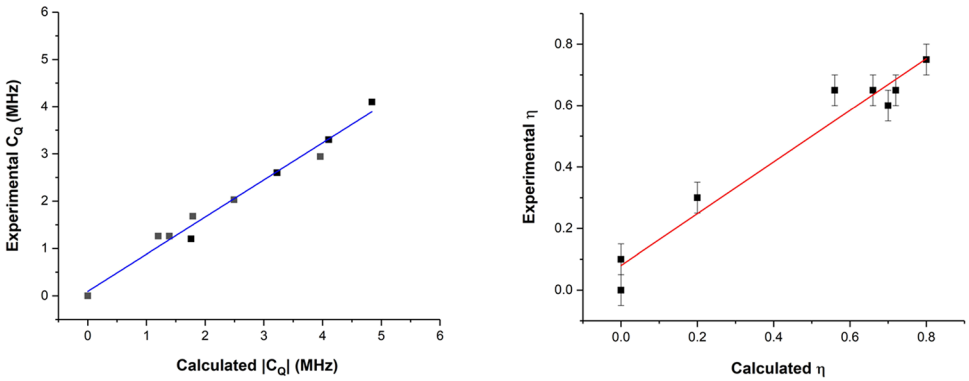

Figure 3. Comparison between Experimental and DFT-calculated values of ^{95}Mo C_Q (left) and η (right) of MoO_4 and MoO_6 sites in various molybdate compounds listed in Table 1. Straight lines through data points represent linear least-squares fits given by eqs 3 and 4 in the text.

The Brillouin zone was sampled using the Monkhorst−Pack scheme and a 4 × 4 × 4 *k*-point grid. The EFG tensor was calculated from the second spatial derivative of the electrostatic potential resulting from the charge density in the crystal. The principal components of this tensor $V_{zz} \geq V_{yy} \geq V_{xx}$ yield the C_Q and η parameters as follows:

$$C_Q = eQV_{zz}/h \tag{1}$$

$$\eta = \frac{V_{xx} - V_{yy}}{V_{zz}} \tag{2}$$

In eq 1 *e* is the electronic charge, *h* is Planck's constant, and *Q* is the quadrupole moment of ^{95}Mo (−22 mB). Calculations were carried out on molybdate crystal structures reported in the literature, with and without geometry optimization. In all cases geometry optimization did not seem to have a significant effect on the resulting quadrupolar parameters. Therefore, here we report the DFT results on unoptimized structures (Table 1). Preliminary attempts of calculating ^{95}Mo magnetic shielding tensors for these crystalline compounds yielded unreliable results at this level of DFT without the consideration of relativistic effects and were not pursued further in the present study. It is to be noted that previous studies in the literature[34] demonstrated the importance of the inclusion of relativistic effects in the DFT calculations for accurate estimation of the large paramagnetic component of ^{95}Mo chemical shift that arises from a symmetry-allowed mixing of occupied and virtual d-orbitals of this transition metal.

The C_Q and η values obtained for the compounds $BaMoO_4$, $PbMoO_4$, and $CaMoO_4$ are found to be in good agreement with those reported in a previous study where the calculations were carried out employing the linearized augmented plane wave + local orbitals (L/APW+lo) method using the code WIEN2k.[18] A comparison between the experimental and DFT-calculated $|C_Q|$ and η values indicates approximate linear correlation with 15−20% overprediction (Figure 3) that can be described using the following relationships ($R^2 \sim 0.95$):

$$C_Q^{expt} = 0.80 \times C_Q^{calc} + 0.09 \tag{3}$$

and

$$\eta^{expt} = 0.84 \times \eta^{calc} + 0.08 \tag{4}$$

The superscripts expt and calc in eqs 3 and 4 correspond, respectively, to experimental and calculated values of $|C_Q|$ and η. It is interesting to note that quite similar functional relationships as in eqs 3 and 4 were also obtained in a recent study of ^{95}Mo NMR parameters on a wide range of molybdates, where the authors utilized a higher cutoff energy of 700 eV for the plane wave basis sets and a more stringent

https://doi.org/10.1021/acs.jpcc.5c00614
J. Phys. Chem. C 2025, 129, 6869−6881

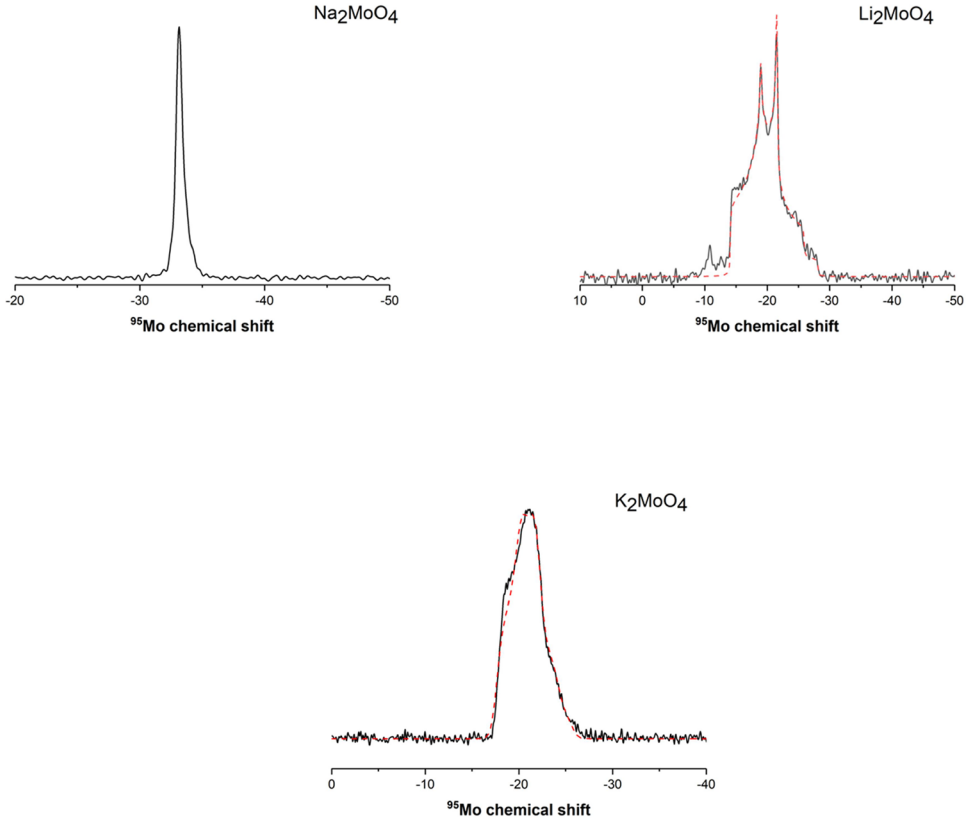

Figure 4. Experimental ^{95}Mo MAS NMR spectra (black solid lines) of alkali orthomolybdate crystals. Spectrum of Na_2MoO_4 was collected at 18.8 T while the spectra of Li_2MoO_4 and K_2MoO_4 were collected at 20.0 T. Simulated spectra of K_2MoO_4 and Li_2MoO_4 are shown as red dashed lines.

Table 2. ^{95}Mo NMR Parameters for Octahedral Mo Environments in Crystalline Alkali Orthomolybdate and Pyromolybdate Compounds Obtained from Simulation of ^{95}Mo MAS NMR Spectra Acquired in This Study

composition	Mo site	Mo−O range (average) Å	σ (°)	δ_{iso} (±0.5 ppm)	C_Q (±0.05 MHz)	η (±0.05)
Na_2MoO_4	tetrahedral	1.788	0.00	−33.5	0.0	
Li_2MoO_4	tetrahedral	1.759−1.769 (1.76)	1.40	−26.0	1.25	0.65
K_2MoO_4	tetrahedral	1.742−1.785 (1.76)	1.68	−17.5	1.26	0.65
$Na_2Mo_2O_7$	tetrahedral	1.708−1.784 (1.76)	1.46	−25.0	1.20	0.70
	octahedral	1.685−2.267 (1.95)	9.76	−11.0	4.10	0.80
$K_2Mo_2O_7$	tetrahedral	1.701−1.837 (1.76)	2.78	−20.0	2.60	0.30
	octahedral	1.725−2.262 (1.97)	10.58	47.0	3.30	0.65

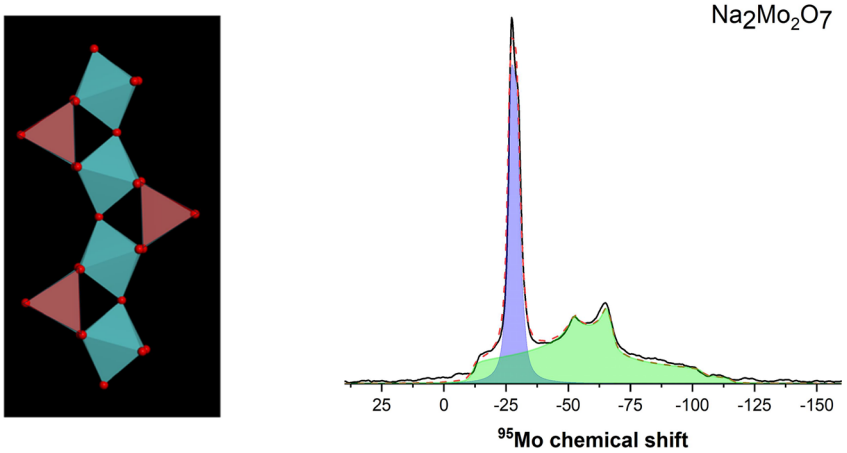

Figure 5. Left: Connectivity of MoO_6 octahedra (teal) and MoO_4 tetrahedra (brown) in the crystal structure of $Na_2Mo_2O_7$. Right: Experimental (black solid line) and simulated (red dashed lines) ^{95}Mo MAS NMR spectra of $Na_2Mo_2O_7$ crystal. Individual simulation components are shown as blue and green shaded peaks.

https://doi.org/10.1021/acs.jpcc.5c00614
J. Phys. Chem. C 2025, 129, 6869−6881

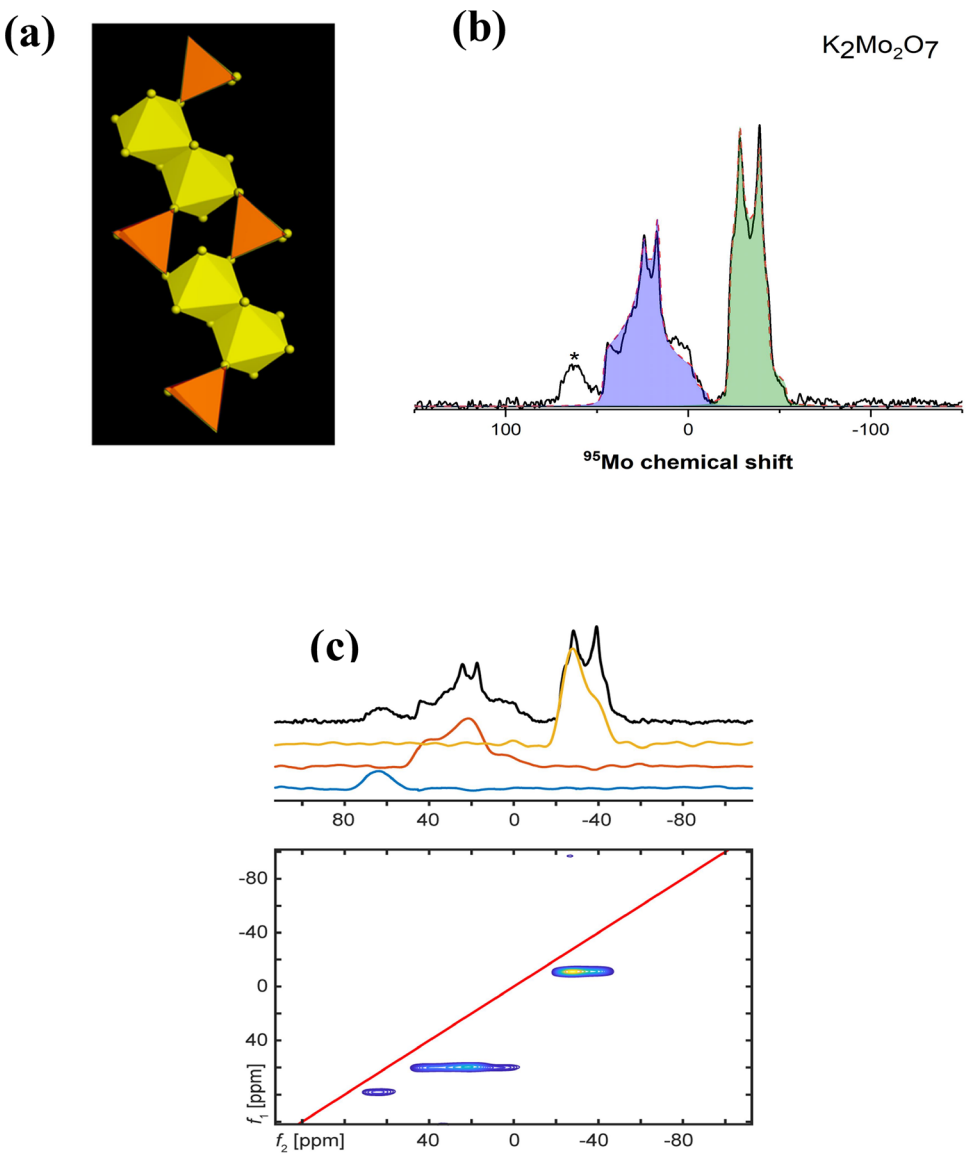

Figure 6. (a) Connectivity of MoO_6 octahedra (yellow) and MoO_4 tetrahedra (orange) in the crystal structure of $K_2Mo_2O_7$. (b) Experimental (black solid line) and simulated (red dashed lines) ^{95}Mo MAS NMR spectra of $K_2Mo_2O_7$ crystal. Individual simulation components are shown as blue and green shaded peaks. Peak with asterisk corresponds to a secondary phase. (c) Contour plot of ^{95}Mo MQMAS NMR spectrum of $K_2Mo_2O_7$ crystal. A comparison between MAS spectrum (black line) and MAS projections of the individual resonances in the MQMAS spectrum is shown on top.

energy convergence criterion of 10^{-8} eV/atom as implemented in the code VASP.[35,36]

3. RESULTS AND DISCUSSION

3.1. Alkali Orthomolybdates. The ^{95}Mo MAS NMR spectra of three A_2MoO_4 phases (A = Li, Na and K) were collected to check for consistency with previously reported data in the literature (Figure 4). The values of δ_{iso}, C_Q, and η obtained from simulation of these spectral line shapes carried out using the software Dmfit (Figure 4) are reported in Table 2. These values are found to be consistent with those reported in previous studies based on simulation of spectra collected at magnetic fields ranging between and 11.7 and 19.6 T.[18−20] As noted earlier, the MoO_4 tetrahedra in these compounds are rather regular with a small spread in Mo−O bond distances and Mo−O−Mo angles. The perfect T_d symmetry of the MoO_4 tetrahedron in Na_2MoO_4[37] resulted in a symmetric line shape with negligible quadrupolar broadening, i.e., $C_Q \approx 0$ MHz.[18,19] The MoO_4 tetrahedra in Li_2MoO_4 and K_2MoO_4 show small departure from tetrahedral symmetry[38,39] with similar bond angle distortion parameters ($\sigma \sim 1.40-1.68$), which results in relatively low C_Q values for these Mo sites (1.25−1.26 MHz, see Table 2). The average Mo−O bond distances for the Na, Li, and K phases are 1.788, 1.764, and 1.762 Å, respectively. On the other hand, the δ_{iso} for the Na, Li, and K phases are −33.5, −26.0, and −17.5 ppm, respectively, implying the lack of any clear correlation between δ_{iso} and Mo−O bond distance (Table 2), as was noted in previous studies.[18,19]

3.2. Na and K Pyromolybdates. The structure of the $Na_2Mo_2O_7$ phase is characterized by chains of corner-shared MoO_6 octahedra along the *a*-axis where pairs of adjacent octahedra share corners with a MoO_4 tetrahedron,[40] resulting in octahedral and tetrahedral Mo sites being present in 1:1

https://doi.org/10.1021/acs.jpcc.5c00614
J. Phys. Chem. C 2025, 129, 6869−6881

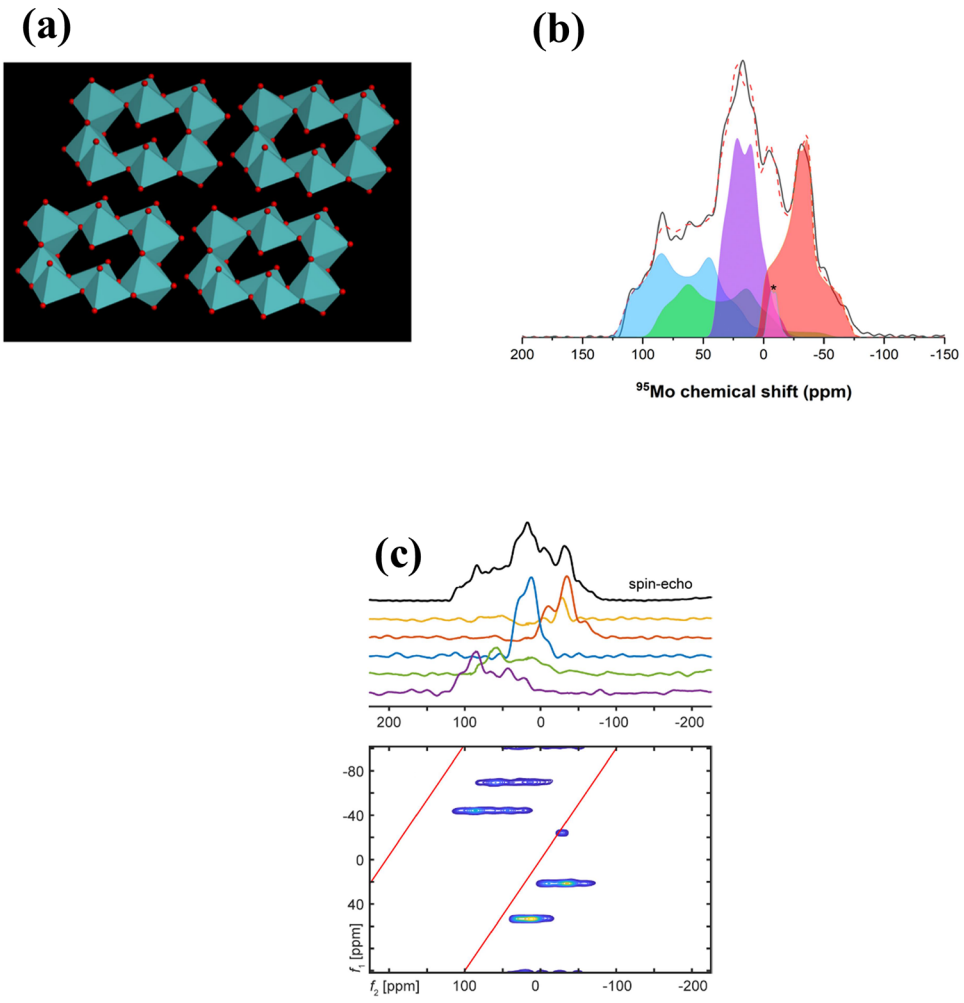

Figure 7. (a) Connectivity of MoO_6 octahedra in the structure of $Li_4Mo_5O_{17}$ crystal showing groups of 10 MoO_6 octahedra sharing edges to form ribbons along *b* direction. (b) Experimental (black solid line) and simulated (red dashed lines) ^{95}Mo MAS NMR spectra of $Li_4Mo_5O_{17}$ crystal. Individual simulation components are shown as colored shaded peaks. Peak with asterisk corresponds to a secondary phase. (c) Contour plot of ^{95}Mo MQMAS NMR spectrum of $Li_4Mo_5O_{17}$ crystal. A comparison between MAS spectrum (black line) and MAS projections of the individual resonances in the MQMAS spectrum is shown on top.

ratio (Figure 5). The Mo−O bond distances (1.71−1.78 Å with an average of 1.76 Å) and the angular distortion parameter σ (∼1.46) for the MoO_4 tetrahedra in this structure are quite similar to those observed in orthomolybdates (Table 2). In contrast, the MoO_6 octahedra in this structure are highly distorted with Mo−O bond distances ranging between 1.69 and 2.27 Å (average Mo−O of 1.95 Å) and a rather large σ (∼9.8). The experimental ^{95}Mo MAS NMR spectrum (Figure 5) displays two partially overlapping but clear quadrupolar powder patterns corresponding to these two environments. Simulation of this spectrum (Figure 5) yields for the narrower resonance: δ_{iso} = −25 ppm, C_Q = 1.2 MHz, and η = 0.70, while for the broader resonance we obtained: δ_{iso} = −11 ppm, C_Q = 4.1 MHz, and η = 0.80 (Table 2). The peak areas suggest that these two Mo environments are indeed present in equal abundance in the structure of $Na_2Mo_2O_7$. It may be noted here that the narrower resonance was also observed in a previous study by Wren et al.,[19] however, the relatively low magnetic fields of 9.4 and 14.1 T used in that study failed to clearly resolve the broader second resonance. The equal abundance of the two environments makes their identification somewhat challenging in the ^{95}Mo NMR spectrum (Figure 5). However, it may seem logical to assign the resonance at δ_{iso} = −11 ppm, characterized by the rather large C_Q to the MoO_6 environment, which is highly distorted with a large spread in the Mo−O distances and a high value of σ (Table 2). Moreover, the Mo−O spread and the σ value of the MoO_4 environment of $Na_2Mo_2O_7$ is consistent with the C_Q of the resonance centered at δ_{iso} = −25 ppm.[19] Therefore, we assign the resonance at δ_{iso} = −25 ppm to the tetrahedral Mo site and the resonance at δ_{iso} = −11 ppm to the octahedral Mo site. This assignment is completely consistent with the results of the DFT calculations that yield a significantly higher C_Q value (3.3 MHz) for the octahedral environment compared to that (1.2 MHz) for the tetrahedral environment (Table 1).

The structure of the $K_2Mo_2O_7$ phase is characterized by pairs of edge-shared MoO_6 octahedra connected via corner-sharing pairs of opposing MoO_4 tetrahedra forming chains along the *b*-axis,[41] again resulting in an equal abundance of octahedral and tetrahedral Mo sites (Figure 6a). The Mo−O bond distances in the MoO_4 tetrahedra vary over a wider range (∼1.70−1.84 Å) in this structure and display a significantly larger σ (∼2.78), compared to those characteristic of its Na analogue. The edge-shared octahedral environment in $K_2Mo_2O_7$ on the other hand, is characterized by Mo−O distances ranging between 1.73 and 2.26 Å and σ ∼ 10.6, both

https://doi.org/10.1021/acs.jpcc.5c00614
J. Phys. Chem. C 2025, 129, 6869−6881

Table 3. ^{95}Mo NMR Parameters for Octahedral Mo Environments in Crystalline Li-Polymolybdate Compound $Li_4Mo_5O_{17}$, Obtained from Simulation of ^{95}Mo MAS and MQMAS Spectra Acquired in This Study

composition	Mo site	Mo−O range (average) Å	σ	δ_{iso} (±0.5 ppm)	C_Q (±0.05 MHz)	η (±0.05)
$Li_4Mo_5O_{17}$	octahedral	1.688−2.497 (1.95−1.97)	∼9.5	124.0	5.38	0.39
	octahedral			99.4	5.55	0.31
	octahedral			40.3	3.37	0.50
	octahedral			2.1	3.73	0.79

being comparable to those observed for the MoO_6 site in the structure of $Na_2Mo_2O_7$. The ^{95}Mo MAS NMR spectrum of $K_2Mo_2O_7$ (Figure 6b) displays two well-resolved quadrupolar powder patterns corresponding to these two environments. Simulation of this spectrum yields for the narrower resonance: δ_{iso} = −20 ppm, C_Q = 2.6 MHz, and η = 0.30, while the broader resonance can be simulated using δ_{iso} = 47 ppm, C_Q = 3.3 MHz, and η = 0.65 (Table 2). The C_Q of the narrower resonance is consistent with the σ for the MoO_4 tetrahedral sites in $K_2Mo_2O_7$ and falls on the extrapolated linear trend between C_Q and σ for the MoO_4 tetrahedral sites that was reported by Wren et al.[19] in a previous ^{95}Mo MAS NMR study of alkali molybdates. Similar to the spectrum of $Na_2Mo_2O_7$, we assign the resonance with smaller C_Q and η in the ^{95}Mo MAS NMR spectrum of $K_2Mo_2O_7$ to the tetrahedral site and the broader resonance to the octahedral site. Again, the DFT calculations are observed to be in complete agreement with this assignment, predicting a lower C_Q (2.2 MHz) for the tetrahedral site, compared to that (2.8 MHz) for the octahedral site (Table 1). Finally, we note the presence of a relatively weak (∼8%) signal centered at ∼63 ppm in the ^{95}Mo MAS NMR spectrum of $K_2Mo_2O_7$ associated with the presence of a small amount of an additional phase formed during its synthesis, as was also observed in the X-ray diffraction pattern. The ^{95}Mo MQMAS/QCPMG NMR spectrum of $K_2Mo_2O_7$ is shown in Figure 6c. The Mo resonances of the tetrahedral and octahedral Mo sites are clearly resolved in the isotropic dimension, implying excellent feasibility of such experiments in future for high-resolution ^{95}Mo NMR in solids.

The result of a high-coordinated cation site in these alkali pyromolybdates being characterized by a higher value of δ_{iso} and C_Q compared to a low-coordinated site may seem somewhat counterintuitive at first, since an opposite trend is typically observed for nearly all other nuclides in oxides (e.g., ^{23}Na, ^{27}Al, ^{11}B, ^{7}Li, ^{25} Mg, ^{29}Si, ^{31}P, ^{43}Ca, ^{45}Sc, and even the heavy element ^{89}Y) in oxides.[42] A similar observation was also made in recent DFT calculations by Yasui et al. of NMR parameters of tetrahedral and octahedral Mo sites in the perovskite $Ba_7Nb_4MoO_{20}$, where the latter sites are characterized by higher values of δ_{iso} and C_Q.[36] However, before considering these trends in the ^{95}Mo NMR parameters to be anomalous, one needs to consider the unusually large spread of Mo−O distances with a bimodal distribution for the corner- and edge-shared MoO_6 environments in these alkali pyromolybdate compounds. Typically, two of the six Mo−O bonds in these MoO_6 octahedra are longer than 2.2 Å while the other four range between ∼1.7 and 1.9 Å.[40,41] Therefore, these MoO_6 octahedra can be considered as MoO_4 tetrahedra, if an Mo−O distance of >2.0 Å is considered as the cutoff for bonding interactions. A similar situation exists for the crystal structure of molybdite (MoO_3), which can be described in terms of layers of corner- and edge- shared MoO_6 octahedra or alternatively, upon considering a cutoff distance of ≥2.25 Å for the Mo−O bonding interaction, this structure can also be described as parallel chains of corner-shared MoO_4 tetrahedra along the c-axis.[43] A similar cutoff distance leads to a description of the structure of $Na_2Mo_2O_7$ in terms of isolated MoO_4 tetrahedra and corner-sharing MoO_4 tetrahedra, and of the structure of $K_2Mo_2O_7$ in terms of isolated tetrahedra and dimers. The possible effect of such distortion on the ^{95}Mo δ_{iso} is discussed in more detail in the following section.

3.3. Li Polymolybdate $Li_4Mo_5O_{17}$. The structure of the polymolybdate phase $Li_4Mo_5O_{17}$ is described as a complex network of highly distorted edge-shared MoO_6 octahedra that are interlinked via LiO_4 and LiO_6 octahedra.[23,44,45] In particular, the structure can be considered to consist of groups of 10 MoO_6 octahedra sharing edges to form ribbons (Figure 7a). These ribbons are linked together by LiO_4 and LiO_6 polyhedra. The ^{95}Mo MAS NMR spectrum of $Li_4Mo_5O_{17}$ (Figure 7b) displays a line shape consisting of strongly overlapping signals from multiple Mo sites. The ^{95}Mo MQMAS/QCPMG NMR spectrum of this compound (Figure 7c) shows clear resolution of at least four Mo sites in the isotropic dimension along with a relatively weak resonance corresponding likely to small amounts of a secondary phase in this sample. The δ_{iso} and the quadrupolar product $P_Q = C_Q(1 + \eta^2/3)$ for these resonances for a spin $I = 5/2$ nuclide such as ^{95}Mo can be estimated from their isotropic peak position δ_{F_1} and their center of gravity $\delta_{F_2}^{CG}$ along the MAS dimension in the MQMAS spectrum using the following relations:

$$\delta_{iso} = \frac{17}{27}\delta_{F_1} + \frac{10}{27}\delta_{F_2}^{CG} \quad (5)$$

$$P_Q = [(\delta_{F_1} - \delta_{F_2}^{CG})^{1/2}]\left(\frac{\nu_0}{1000}\right)\sqrt{\frac{680[2I(2I-1)]^2}{81[4I(I+1)-3]}} \quad (6)$$

where ν_0 is the resonance frequency (55.4 MHz) and $I = 5/2$ is the spin quantum number of the nuclide. Using these relations, one can obtain the δ_{iso} and P_Q values for the four resolved ^{95}Mo resonances in the MQMAS spectrum corresponding to the $Li_4Mo_5O_{17}$ phase, which are then used to simulate the MAS line shape as shown in Figure 7b. The resulting ^{95}Mo NMR parameters are listed in Table 3.

Structural refinement based on X-ray diffraction suggests that Mo atoms in this compound are present in five crystallographically different environments with Mo−O distances ranging between ∼1.688 and 2.497 Å and average Mo−O distances in these octahedra ranging between 1.96 and 1.98 Å. These values are similar to those reported for the MoO_6 octahedra in Na and K-pyromolybdates (Table 2). It may be noted that the Mo−O distances for at least two of these 5 Mo sites (Mo2 and Mo5) are rather similar. Moreover, an Mo−O bonding cutoff distance of ∼2.2 would render several of these sites 5-fold or even 4-fold coordinated to oxygen. Considering this complexity in the bonding Mo−O environment, we do not attempt any structural assignment of the four resonances in the ^{95}Mo NMR spectra. Rather we

https://doi.org/10.1021/acs.jpcc.5c00614
J. Phys. Chem. C 2025, 129, 6869−6881

simply note that ^{95}Mo MQMAS NMR can be highly effective in resolving strongly overlapping signal in regular MAS spectra from multiple crystallographically similar local environments in a structurally complex compound. Nevertheless, the quadrupolar parameters C_Q and η for these Mo sites as calculated using DFT (Table 1) indeed agree reasonably well with those obtained from the simulation of the ^{95}Mo MAS NMR line shape (Figure 7b, Table3).

As noted earlier, previous high resolution ^{95}Mo MAS NMR spectroscopic studies of molybdate compounds failed to observe any clear correlation between the ^{95}Mo δ_{iso} and the Mo−O bond length or coordination number.[18,19] However, within a limited set of compounds such as the single-alkali orthomolybdates, the ^{95}Mo δ_{iso} for the MoO_4 tetrahedral environment was found to vary within a relatively narrow range of −17 to −34 ppm. The δ_{iso} for the MoO_4 sites in the Na and K pyromolybdates studied here is observed to fall within this range as well. Interestingly, this chemical shift range for tetrahedral Mo extends further to lower frequencies when one includes the reported ^{95}Mo δ_{iso} of −125 ppm for the MoO_4 site in the mixed-alkali orthomolybdate $CsLiMoO_4$.[46] This chemical shift range for tetrahedral Mo is consistent the observed ^{95}Mo δ_{iso} of −73 ppm for molybdite (MoO_3), if one considers the Mo to be four-coordinated in this compound. On the other hand, the ^{95}Mo δ_{iso} for the MoO_6 and $Mo_{5+\delta}$ sites with similar Mo−O bond length ranges (~1.7 to 2.3 Å) and average Mo−O distances (1.95−1.98 Å) in Na- and K-pyromolybdates and in the Li-polymolybdate phases are higher and range between −11 and 124 ppm (Tables 2 and 3). When taken together, these NMR results on a variety of alkali molybdates suggest that the $Mo_{5+\delta}$ and MoO_6 sites are characterized by higher values of δ_{iso} than those characteristic of the MoO_4 sites. A similar observation has also been made in recent ^{95}Mo NMR spectroscopic studies and DFT calculations by Yasui et al. and Tansho et al. on Ba−Nb−W-molybdate perovskites.[35,36] The shielding of a nuclear spin and hence, its chemical shift is a sum of a diamagnetic and a paramagnetic component. The diamagnetic component is typically larger and decreases the chemical shift but is controlled by the core electrons, while the paramagnetic component increases the chemical shift. As the latter is controlled by the valence electrons, the paramagnetic shift is most sensitive to the bonding environment of the nuclide. In the vast majority of cases, an increase in the coordination number results in a lengthening of the metal−ligand bond (e.g., metal−oxygen M−O bonds in an oxide), which lowers the electron density at the metal nuclide and consequently the chemical shift decreases (or shielding increases). The opposite trend observed in the present study for ^{95}Mo in alkali molybdates may be explained as follows. The Mo^{6+} (d^0 electronic state) in MoO_6 octahedra is known to be somewhat unique among transition metals in the sense that these octahedra undergo large distortions, often characterized by a trimodal Mo−O bond length distribution centered at ~1.7, 1.9, and 2.3 Å, when Mo−O−Mo linking is present via corner or edge- sharing between MoO_6 polyhedra.[47] Such large distortions have been shown to arise from both bond topological constraints associated with a lowering of crystallographic symmetry as well as from electronic effects such as the pseudo- or second-order Jahn−Teller distortion [ref].[47−49] The latter leads to a strong overlap and mixing between oxygen 2p orbitals at the top of the valence band (HOMO) and the transition metal t_{2g} orbitals at the bottom of the conduction band (LUMO),[47−49] which is expected to amplify the paramagnetic component of the chemical shift and thus may increase the δ_{iso} of MoO_6 sites. This increase in δ_{iso} could be further amplified due to a distortion-induced increase in the chemical shift anisotropy if the effect of the paramagnetic deshielding is the strongest for the least shielded component. Finally, we note that similar to the observation made by Wren et al.[19] in a previous study on a limited set of alkali molybdates, an approximately linear increase in C_Q with σ is observed in the present study for the MoO_4 tetrahedral sites in both alkali ortho- and pyro-molybdates (Figure 8). Moreover, MoO_4 sites in other orthomolybdates such as $BaMoO_4$, $PbMoO_4$, and $CaMoO_4$ appear to obey the same functional relationship between C_Q and σ (Figure 8). However, no clear correlation between these two quantities is observed for the high-coordinated Mo sites in alkali pyro- and poly-molybdates studied here (Tables 2 and 3).

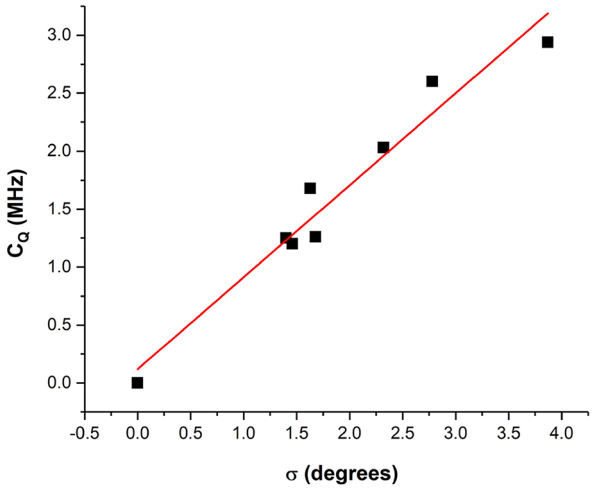

Figure 8. Variation of ^{95}Mo C_Q with tetrahedral distortion parameter σ for MoO_4 sites in ortho- and pyro-molybdate compounds listed in Table 1. Straight line through the data points is a linear least-squares fit given by the relation: $C_Q = 0.79 \times \sigma + 0.12$.

3.4. Mixed-Alkali Molybdate Glasses. The ^{95}Mo MAS NMR spectra of the two alkali molybdate glasses Mo-60 and Mo-62.5 are shown in Figure 9a,b. These spectra display a rather broad and asymmetric line shape with a tail on the high frequency side (higher ppm values). The ^{95}Mo MQMAS/QCPMG NMR of the Mo-62.5 glass clearly indicate the presence of at least two resonances (Figure 9c). The orientation of the contours of the stronger resonance centered near −25 ppm implies a Mo site with a rather small P_Q, that is spectrally broadened predominantly from a chemical shift distribution. On the other hand, the weaker resonance appears to have a higher degree of quadrupolar broadening and its location in the MQMAS spectrum yields δ_{iso} ~ 28 ppm and P_Q ~ 2.5 MHz from eqs 5 and 6. The corresponding quadrupolar broadening of the line shape for this resonance at this magnetic field would be on the order of ~25 ppm, which justifies the simulation of the asymmetric line shapes of the ^{95}Mo MAS NMR spectrum with two broad Gaussian peaks with $\delta_{iso} = -26 \pm 2$ and 28 ± 2 ppm and full-width-at-half-maximum (fwhm) of 60 ppm, as shown in Figure 9b. This simulation yields a ratio of ~85:15 for the two Mo sites with $\delta_{iso} = -26 \pm 2$ and 28 ± 2 ppm, respectively, in the Mo-60 glass. The ^{95}Mo MAS NMR spectrum of the Mo-62.5 glass can similarly be simulated

https://doi.org/10.1021/acs.jpcc.5c00614
J. Phys. Chem. C 2025, 129, 6869−6881

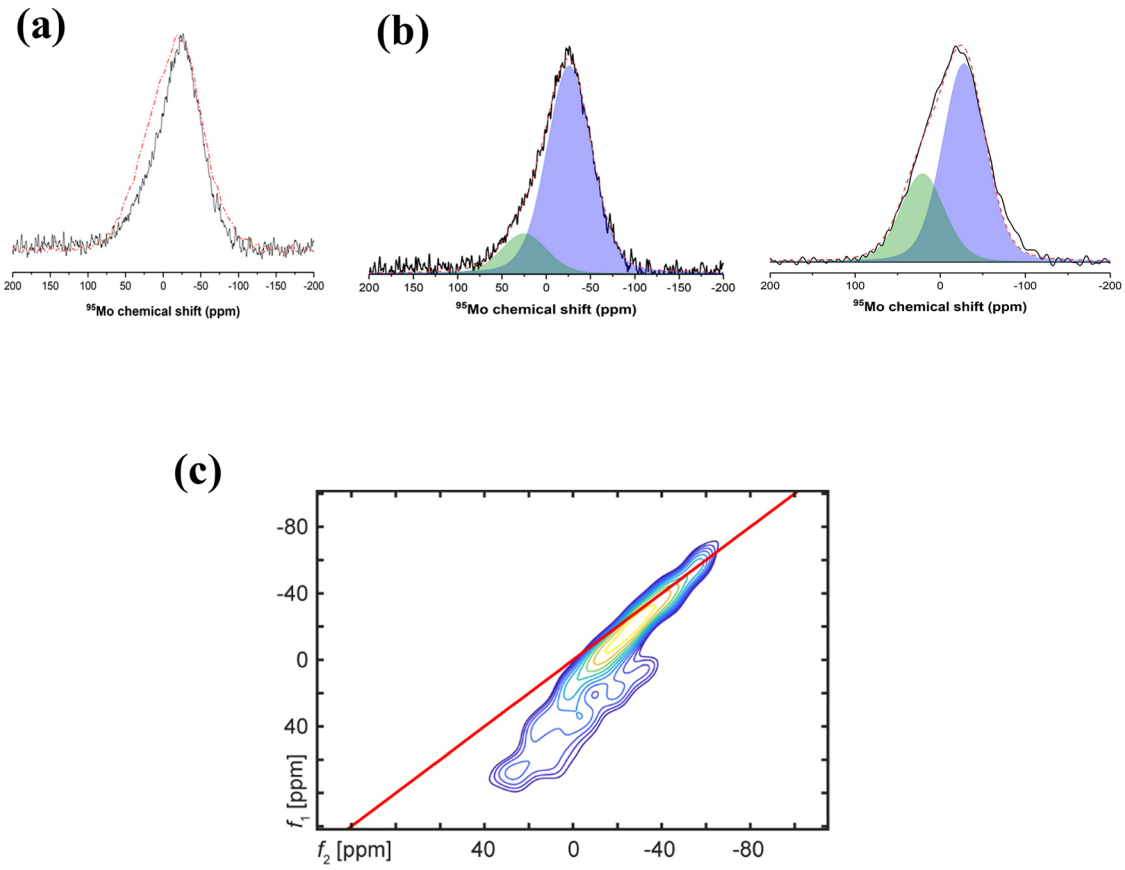

Figure 9. (a) Overlay plot of ^{95}Mo MAS NMR spectra of Mo-60 (solid line) and Mo-62.5 (dot-dashed line) glasses. (b) Experimental (black solid line) and simulated (red dashed lines) ^{95}Mo MAS NMR spectra of Mo-60 (left) and Mo-62.5 (right) glasses. Individual simulation components corresponding to MoO_4 and MoO_6 sites are shown as blue and green shaded peaks, respectively. (c) Contour plot of ^{95}Mo MQMAS/QCPMG NMR spectra of Mo-62.5 glass displaying a strong and a weak resonance corresponding, respectively, to MoO_4 and MoO_6 sites.

with two Gaussian peaks with the same fwhm and similar δ_{iso} = −27 ± 2 and 23 ± 2 ppm with a relative ratio of 70:30 (Figure 9b). The presence of more than one type of Mo−O coordination environment in these glasses was also reported in a recent study based on Raman spectroscopy, which suggested a coexistence of MoO_4 tetrahedra and MoO_6 octahedra in the structure of these alkali molybdate glasses.[7] More specifically, the structure of glasses with ≤55% MO_3 was found in this study to be dominated by isolated $[MO_4]^{2-}$ tetrahedra, while the Raman spectra of glasses with higher MO_3 content such as the ones studied here were interpreted to indicate the formation of chain-like moieties of corner- and edge- sharing MO_6 octahedra and MO_4 tetrahedra. Considering the lack of a clear chemical shift systematics, a structural assignment of the two ^{95}Mo resonances in Figure 9 cannot be made solely on the basis of their differences in P_Q. However, the δ_{iso} and small P_Q of the stronger resonance are indeed similar to those that are characteristic of the MoO_4 tetrahedral sites in a variety of alkali ortho- and pyro-molybdates, as shown in the present study (Table 2). On the other hand, the δ_{iso} of the weaker resonance (23−28 ppm) falls within the range (−11 to 124 ppm) observed in this study for the MoO_6 and $Mo_{5+\delta}$ sites sites in Na- and K-pyromolybdate and in the Li-polymolybdate compounds. Therefore, we tentatively assign the stronger resonance to the MoO_4 tetrahedral environment and the weaker resonance to the high-coordinated MoO_6/$Mo_{5+\delta}$ environment in the structure of alkali molybdate glasses. Simulations presented in Figure 9b indicate that the relative fraction of the latter environment increases from ∼15 to ∼30% upon increasing the Mo content in these glasses. This trend is consistent with the results of a previous Raman spectroscopic study,[7] which indicated the tetrahedral environment to be more abundant than the octahedral environment in these glasses and the relative fraction of the latter increased with Mo content.

3.5. Implications for the Local Structure around Mo in Nuclear Waste Glasses. Molybdenum serves as an important constituent in various structural components in nuclear reactors where its oxidation results in significant concentration of MoO_3 in the high-level liquid waste (HLW) produced by the reprocessing of the spent fuel.[50] The HLW is typically immobilized and stored via vitrification in a borosilicate glass matrix. However, the low solubility of Mo in the borosilicate glass network may result in phase separation and crystallization of various alkali molybdates in the so-called yellow phase that can negatively impact the durability of the encapsulated waste form.[50−52] Majority of the applications of ^{95}Mo NMR spectroscopy therefore focused on the characterization of these crystalline alkali molybdate phases in typical Na−Ca-borosilicate glass matrices.[51,52] There has, however, been one systematic study in the literature of the Mo environment in borosilicate glasses by Magnin et al. that utilized ^{95}Mo MAS NMR at a magnetic field of 18.8 T.[53] These spectra are characterized by broad and unresolved line shapes where the broadening cannot be conclusively attributed to quadrupolar or chemical shift distribution effects. The center

https://doi.org/10.1021/acs.jpcc.5c00614
J. Phys. Chem. C 2025, 129, 6869−6881

of gravity of the ^{95}Mo MAS NMR line shape was found to systematically shift upfield to more negative chemical shift values on progressive replacement of Na with Ca as the network modifying cation. These spectra were a priori assigned to $[MoO_4]^{-2}$ tetrahedral species on the basis of previous a Mo K-edge EXAFS study[54] and the authors argued that these tetrahedra, when charge balanced by Ca cations resulted in a more negative chemical shift (e.g., −50 ppm) compared to when charge balanced by Na cations (e.g., −5 ppm) in the glass structure.[53] At first glance this chemical shift trend is at odds with the fact that the ^{95}Mo δ_{iso} of $CaMoO_4$ is ∼80 ppm higher than that of Na_2MoO_4. However, the ^{95}Mo δ_{iso} has been shown to be highly sensitive to the number and type of charge balancing cations that share the oxygen with the Mo−O polyhedra. The low solubility of Mo in the borosilicate glass has been associated in the literature with the formation of isolated $[MoO_4]^{-2}$ tetrahedra, which would scavenge the alkali and alkaline-earth cations from the structure of the host glass to phase separate and eventually form the so-called yellow phase.[51,52] However, an increased solubility of Mo on replacement of Si with P in such glasses has been hypothesized to be related to the formation of MoO_6 octahedra that can be connected to the PO_4 tetrahedra via Mo−O−P linkages in the glass structure.[52] The results presented in this study indicate that such a mechanism of Mo dissolution may be investigated in future using high-field and high-resolution ^{95}Mo NMR spectroscopy.

4. SUMMARY

High-resolution ^{95}Mo MAS and MQMAS NMR spectra of crystalline anhydrous alkali ortho-, pyro-, and poly-molybdates in combination with DFT-based calculations provide distinct ^{95}Mo δ_{iso} ranges of −17 to −125 ppm for MoO_4 and of −11 to 124 ppm for MoO_6 coordination environments, respectively. The corresponding C_Q values are found to be ≤2.6 MHz for MoO_4 and ≥3.3 MHz for MoO_6 sites. These apparently anomalous trends of higher δ_{iso} and C_Q for a high-coordinated site are tentatively linked to the highly distorted geometry of MoO_6 octahedra in corner- and edge-shared configuration in these molybdates that results in an increase in the paramagnetic component of the ^{95}Mo chemical shift. However, detailed DFT based calculations will need to be carried out in future to critically test this hypothesis. The MoO_4 tetrahedral sites display an approximately linear increase in C_Q with σ, while no such correlation is observed for the high-coordinated Mo sites. The ^{95}Mo MAS and MQMAS NMR spectra indicate that tetrahedral and octahedral Mo−O environments coexist in alkali molybdate glasses and the MoO_6:MoO_4 ratio increases with increasing MoO_3 content. The results presented in this study may have important implications in the future applications of high-resolution ^{95}Mo NMR spectroscopy in probing the Mo coordination environment and its dissolution mechanism in nuclear waste glasses.

AUTHOR INFORMATION

Corresponding Author

Sabyasachi Sen − *Department of Materials Science and Engineering, University of California at Davis, Davis, California 95616, United States;* orcid.org/0000-0002-4504-3632; Email: sbsen@ucdavis.edu

Authors

Ivan Hung − *National High Magnetic Field Laboratory, Tallahassee, Florida 32310, United States;* orcid.org/0000-0001-8916-739X

Jacob M. Lovi − *Department of Materials Science and Engineering, University of California at Davis, Davis, California 95616, United States*

Zhehong Gan − *National High Magnetic Field Laboratory, Tallahassee, Florida 32310, United States;* orcid.org/0000-0002-9855-5113

Complete contact information is available at: https://pubs.acs.org/10.1021/acs.jpcc.5c00614

Notes

The authors declare no competing financial interest.

ACKNOWLEDGMENTS

This work was supported by an NSF grant (DMR 2409281) to S.S. The National High Magnetic Field Laboratory is supported by the National Science Foundation through NSF/DMR-2128556 and the State of Florida. Authors acknowledge Martine Monette, Alia Hassan and Jochem Struppe at the Bruker Biospin Group for their assistance with the ^{95}Mo NMR spectral acquisition at 18.8 T using Bruker CPMAS cryoprobe.

REFERENCES

(1) Chen, X. R.; Zhai, Q. J.; Dong, H.; Dai, B. H.; Mohrbacher, H. Molybdenum alloying in cast iron and steel. *Advances in Manufacturing* **2020**, *8*, 3−14.

(2) El-Sharkawy, E. A.; Khder, A. S.; Ahmed, A. I. Structural characterization and catalytic activity of molybdenum oxide supported zirconia catalysts. *Microporous Mesoporous Mater.* **2007**, *102* (1−3), 128−137.

(3) Benck, J. D.; Chen, Z.; Kuritzky, L. Y.; Forman, A. J.; Jaramillo, T. F. Amorphous molybdenum sulfide catalysts for electrochemical hydrogen production: insights into the origin of their catalytic activity. *ACS Catal.* **2012**, *2* (9), 1916−1923.

(4) Van der Wielen, J. T. G.; Stein, H. N.; Stevels, J. M. Glass formation in alkali molybdate systems. *J. Non-Cryst. Solids* **1968**, *1* (1), 18−28.

(5) Baynton, P. L.; Rawson, H.; Stanworth, J. E. Glass Based on the oxides of Molybdenum. *Tungsten and Uranium. Nature* **1956**, *178* (4539), 910−911.

(6) Aitken, B.; Dejneka, M. J., Tungstate, molybdate, vanadate base glasses. U.S. Patent. 6,376,399 B1, April 23, 2002.

(7) Lovi, J.; Sen, S. Structure and rheological behavior of mixed-alkali molybdate and tungstate glasses and liquids. *J. Non-Cryst. Solids* **2024**, *639*, No. 123083.

(8) Machida, S.; Maeda, K.; Katsumata, K. I.; Yasumor, A. Effect of starting materials of nucleation agents on crystallization of CaO−Al2O3−SiO2 glass. *International Journal of Applied Glass Science* **2023**, *14* (1), 88−96.

(9) Machida, N.; Eckert, H. FT-IR, FT-Raman and 95Mo MAS−NMR studies on the structure of ionically conducting glasses in the system AgI−Ag2O−MoO3. *Solid State Ionics* **1998**, *107* (3−4), 255−268.

(10) Poirier, G.; Ottoboni, F. S.; Castro Cassanjes, F.; Remonte, Á.; Messaddeq, Y.; Ribeiro, S. J. L. Redox behavior of molybdenum and tungsten in phosphate glasses. *J. Phys. Chem. B* **2008**, *112* (15), 4481−4487.

(11) Saji, V. S.; Lee, C. W. Molybdenum, molybdenum oxides, and their electrochemistry. *ChemSusChem* **2012**, *5* (7), 1146−1161.

(12) Saraiva, G. D.; Paraguassu, W.; Maczka, M.; Freire, P. T. C.; De Sousa, F. F.; Mendes Filho, J. Temperature-dependent Raman

scattering studies on Na2Mo2O7 disodium dimolybdate. *J. Raman Spectrosc.* **2011**, *42* (5), 1114−1119.
(13) Saraiva, G. D.; Lobato, L. F.; Ferreira, A. V. L.; Paraguassu, W.; de Castro, A. R.; Jucá, R. F.; Neto, V. S.; Teixeira, A. M. R.; Sousa, F. F. A temperature-dependent Raman scattering and X-ray diffraction study of K2Mo2O7·H2O and ab initio calculations of K2Mo2O7. *Spectrochim. Acta, Part A* **2021**, *263*, No. 120184.
(14) Gatehouse, B. M. Alkali metal and silver molybdates and polymolybdates some recently determined structures. *Journal of the Less Common Metals* **1974**, *36* (1−2), 53−59.
(15) Pautonnier, A.; Coste, S.; Barré, M.; Lacorre, P. Higher lanthanum molybdates: Structures, crystal chemistry and properties. *Prog. Solid State Chem.* **2023**, *69*, No. 100382.
(16) Khal'baeva, K. M.; Solodovnikov, S. F.; Khaikina, E. G.; Kadyrova, Y. M.; Solodovnikova, Z. A.; Basovich, O. M. Phase formation features in the systems M2MoO4−Fe2 (MoO4) 3 (M= Rb, Cs) and crystal structures of new double polymolybdates M3FeMo4O15. *J. Solid State Chem.* **2010**, *183* (3), 712−719.
(17) Michailovski, A.; Patzke, G. R. Hydrothermal synthesis and crystal structure of novel alkali trimolybdates. *Zeitschrift für anorganische und allgemeine Chemie* **2007**, *633* (1), 54−62.
(18) d'Espinose de Lacaillerie, J. B.; Barberon, F.; Romanenko, K. V.; Lapina, O. B.; Pollès, L. L.; Gautier, R.; Gan, Z. 95Mo magic angle spinning NMR at high field: improved measurements and structural analysis of the quadrupole interaction in monomolybdates and isopolymolybdates. *J. Phys. Chem. B* **2005**, *109* (29), 14033−14042.
(19) Wren, J. E.; Greer, B. J.; Michaelis, V. K.; Higman, C. S.; Kroeker, S. Multinuclear magnetic resonance investigation of crystalline alkali molybdates. *Inorg. Chem.* **2015**, *54* (20), 9853−9861.
(20) Forgeron, M. A.; Wasylishen, R. E. Molybdenum magnetic shielding and quadrupolar tensors for a series of molybdate salts: a solid-state 95 Mo NMR study. *Phys. Chem. Chem. Phys.* **2008**, *10* (4), 574−581.
(21) Massiot, D.; Montouillout, V.; Magnenet, C.; Bessada, C.; Coutures, J. P.; Forster, H.; Steuernagel, S.; Mueller, D. Towards higher resolution for quadrupolar nuclei in solid state NMR at very high field. *Comptes Rendus de l'Académie des Sciences-Series IIC-Chemistry* **1998**, *1* (3), 157−162.
(22) Gan, Z.; Gor'kov, P.; Cross, T. A.; Samoson, A.; Massiot, D. Seeking higher resolution and sensitivity for NMR of quadrupolar nuclei at ultrahigh magnetic fields. *J. Am. Chem. Soc.* **2002**, *124* (20), 5634−5635.
(23) Solodovnikov, S. F.; Bazarov, B. G.; Pyl'neva, N. A. Li, MoO-MoO, Phase Diagram and Crystal Structure. *Russian J. Inorg. Chem.* **1999**, *44* (6), 954−961.
(24) Dey, K. K.; Prasad, S.; Ash, J. T.; Deschamps, M.; Grandinetti, P. J. Spectral editing in solid-state MAS NMR of quadrupolar nuclei using selective satellite inversion. *J. Magn. Reson.* **2007**, *185* (2), 326−330.
(25) Larsen, F. H.; Jakobsen, H. J.; Ellis, P. D.; Nielsen, N. C. QCPMG-MAS NMR of half-integer quadrupolar nuclei. *J. Magn. Reson.* **1998**, *131* (1), 144−147.
(26) Levitt, M. H.; Madhu, P. K.; Hughes, C. E. Cogwheel phase cycling. *J. Magn. Reson.* **2002**, *155* (2), 300−306.
(27) Brown, S. P.; Wimperis, S. Two-dimensional multiple-quantum MAS NMR of quadrupolar nuclei. Acquisition of the whole echo. *J. Magn. Reson.* **1997**, *124* (1), 279−285.
(28) Brown, S. P.; Heyes, S. J.; Wimperis, S. Two-dimensional MAS multiple-quantum NMR of quadrupolar nuclei. Removal of inhomogeneous second-order broadening. *J. Magn. Res., Ser. A* **1996**, *2* (119), 280−284.
(29) Gan, Z.; Kwak, H. T. Enhancing MQMAS sensitivity using signals from multiple coherence transfer pathways. *J. Magn. Reson.* **2004**, *168* (2), 346−351.
(30) States, D. J.; Haberkorn, R. A.; Ruben, D. J. A two-dimensional nuclear Overhauser experiment with pure absorption phase in four quadrants. *Journal of Magnetic Resonance (1969)* **1982**, *48* (2), 286−292.
(31) Pickard, C. J.; Mauri, F. All-electron magnetic response with pseudopotentials: NMR chemical shifts. *Phys. Rev. B* **2001**, *63* (24), No. 245101.
(32) Yates, J. R.; Pickard, C. J.; Mauri, F. Calculation of NMR chemical shifts for extended systems using ultrasoft pseudopotentials. *Physical Review B—Condensed Matter and Materials. Physics* **2007**, *76* (2), No. 024401.
(33) Bonhomme, C.; Gervais, C.; Babonneau, F.; Coelho, C.; Pourpoint, F.; Azais, T.; Ashbrook, S. E.; Griffin, J. M.; Yates, J. R.; Mauri, F.; et al. First-principles calculation of NMR parameters using the gauge including projector augmented wave method: a chemist's point of view. *Chem. Rev.* **2012**, *112* (11), 5733−5779.
(34) Bryce, D. L.; Wasylishen, R. E. A 95 Mo and 13C solid-state NMR and relativistic DFT investigation of mesitylenetricarbonylmolybdenum (0)−a typical transition metal piano-stool complex. *Phys. Chem. Chem. Phys.* **2002**, *4* (15), 3591−3600.
(35) Tansho, M.; Goto, A.; Ohki, S.; Mogami, Y.; Yasui, Y.; Sakuda, Y.; Fujii, K.; Iijima, T.; Yashima, M. Solid-State 95Mo and 93Nb NMR Study of Ba7Nb4MoO20-Based Materials and Ba7Ta3. 7Mo1. 3O20. 15. *J. Phys. Chem. C* **2024**, *128* (46), 19679−19687.
(36) Yasui, Y.; Tansho, M.; Fujii, K.; Sakuda, Y.; Goto, A.; Ohki, S.; Mogami, Y.; Iijima, T.; Kobayashi, S.; Kawaguchi, S.; et al. Hidden chemical order in disordered Ba7Nb4MoO20 revealed by resonant X-ray diffraction and solid-state NMR. *Nat. Commun.* **2023**, *14* (1), 2337.
(37) Bramnik, K. G.; Ehrenberg, H. Study of the Na2O—MoO3 System. Na6Mo11O36—a New Oxide with Anatase-related Structure, and the Crystal Structures of Na2MoO4. *Zeitschrift für anorganische und allgemeine Chemie* **2004**, *630* (8−9), 1336−1341.
(38) Gatehouse, B. M.; Leverett, P. Crystal structure of potassium molybdate, K 2 MoO 4. *Journal of the Chemical Society A: Inorganic, Physical, Theoretical* **1969**, 849−854.
(39) Kolitsch, U. The crystal structures of phenacite-type Li2 (MoO4), and scheelite-type LiY (MoO4) 2 and LiNd (MoO4) 2. *Zeitschrift für Kristallographie-Crystalline Materials* **2001**, *216* (8), 449−454.
(40) Seleborg, M. A refinement of the crystal structure of disodium dimolybdate. *Acta Chem. Scand.* **1967**, *21*, 499−504.
(41) Zolotova, E. S.; Solodovnikov, S. F.; Solodovnikova, Z. A.; Yudin, V. N.; Uvarov, N. F.; Sukhikh, A. S. Selection of alkali polymolybdates as fluxes for crystallization of double molybdates of alkali metals, zirconium or hafnium, revisited crystal structures of K2Mo2O7, K2Mo3O10, Rb2Mo3O10 and ionic conductivity of A2Mo2O7 and A2Mo3O10 (A= K, Rb, Cs). *J. Phys. Chem. Solids* **2021**, *154*, No. 110054.
(42) MacKenzie, K. J.; Smith, M. E. *Multinuclear solid-state nuclear magnetic resonance of inorganic materials*; vol *6*; Elsevier, 2002.
(43) Kihlborg, L. Least squares refinement of crystal structure of molybdenum trioxide. *Arkiv for Kemi* **1963**, *21* (4), 357.
(44) Wiesmann, M.; Weitzel, H.; Svoboda, I.; Fuess, H. The crystal structure of lithiumpentamolybdate Li4Mo5O17. *Z. Kristallogr.-Crystal. Mater.* **1997**, *212* (11), 795−800.
(45) Grigorieva, V. D.; Kuznetsov, A. B.; Ryadun, A. A.; Kremlev, A. D.; Yudin, V. N.; Shlegel, V. N. Li4Mo5O17 crystal as possible scintillating material: Growth and luminescence properties. *J. Cryst. Growth* **2024**, *627*, No. 127520.
(46) Kroeker, S.; Farnan, I.; Schuller, S.; Advocat, T. 95Mo NMR study of crystallization in model nuclear waste glasses. *MRS Online Proceedings Library (OPL)*, vol *1124*; **2008**; p 1124-Q03-06.
(47) Gagné, O. C.; Hawthorne, F. C. Bond-length distributions for ions bonded to oxygen: Results for the transition metals and quantification of the factors underlying bond-length variation in inorganic solids. *IUCrJ.* **2020**, *7* (4), 581−629.
(48) Ra, H. S.; Ok, K. M.; Halasyamani, P. S. Combining second-order Jahn−Teller distorted cations to create highly efficient SHG materials: synthesis, characterization, and NLO properties of BaTeM2O9 (M= Mo6+ or W6+). *J. Am. Chem. Soc.* **2003**, *125* (26), 7764−7765.

https://doi.org/10.1021/acs.jpcc.5c00614
J. Phys. Chem. C 2025, 129, 6869−6881

(49) Eng, H. W.; Barnes, P. W.; Auer, B. M.; Woodward, P. M. Investigations of the electronic structure of d0 transition metal oxides belonging to the perovskite family. *J. Solid State Chem.* **2003**, *175* (1), 94−109.
(50) Pinet, O.; Hollebecque, J. F.; Hugon, I.; Debono, V.; Campayo, L.; Vallat, C.; Lemaitre, V. Glass ceramic for the vitrification of high level waste with a high molybdenum content. *J. Nucl. Mater.* **2019**, *519*, 121−127.
(51) Krishnamurthy, A.; Nguyen, T.; Fayek, M.; Shabaga, B.; Kroeker, S. Network structure and dissolution properties of phosphate-doped borosilicate glasses. *J. Phys. Chem. C* **2020**, *124* (38), 21184−21196.
(52) Krishnamurthy, A.; Kroeker, S. Improving molybdenum and sulfur vitrification in borosilicate nuclear waste glasses using phosphorus: structural insights from NMR. *Inorganic chemistry* **2022**, *61* (1), 73−85.
(53) Magnin, M.; Schuller, S.; Mercier, C.; Trébosc, J.; Caurant, D.; Majérus, O.; Angéli, F.; Charpentier, T. Modification of molybdenum structural environment in borosilicate glasses with increasing content of boron and calcium oxide by 95Mo MAS NMR. *J. Am. Ceram. Soc.* **2011**, *94* (12), 4274−4282.
(54) Calas, G.; Le Grand, M.; Galoisy, L.; Ghaleb, D. Structural role of molybdenum in nuclear glasses: an EXAFS study. *J. Nucl. Mater.* **2003**, *322* (1), 15−20.

https://doi.org/10.1021/acs.jpcc.5c00614
J. Phys. Chem. C 2025, 129, 6869−6881